Fault Detection and Diagnostics for Non-Intrusive Monitoring using Motor Harmonics

Uzoma A. Orji, Zachary Remscrim, Christopher Laughman, Steven B. Leeb,
Warit Wichakool, Christopher Schantz, Robert Cox,
James Paris, James L. Kirtley, Jr., Les K. Norford

***Abstract*—Harmonic analysis of motor current has been used to track the speed of motors for sensorless control. Algorithms exist that track the speed of a motor given a dedicated stator current measurement, for example [1–5]. Harmonic analysis has also been applied for diagnostic detection of electro-mechanical faults such as damaged bearings and rotor eccentricity [6–17]. This paper demonstrates the utility of harmonic analysis for fault detection and diagnostics in non-intrusive monitoring applications, where multiple loads are tracked by a sensor monitoring only the aggregate utility service. An optimization routine is implemented to maintain accuracy of speed estimation while using shorter lengths of data.**

I. Smart Monitoring

At any point in the life of a system, mechanical and electrical equipment may be poorly operated. For example, as buildings age, both the electro-mechanical actuators and associated mechanical components wear, cease to function properly, and eventually fail, via myriad processes that are often undetected. Valves do not close fully, filters clog, air-conditioning system dampers stick, refrigerant leaks, heating and cooling coils – from the smallest refrigerator to the largest building air-conditioning system – become fouled with dirt and debris, and belts slip. Energy waste and excessive plant wear are often exacerbated by closed-loop control. Under active control, damaged but still functioning equipment will operate by extending run times or operating points to meet user commands, leaving few obvious signs of compromised operation.

For example, a number of surveys of airflow faults in buildings hint at the range and extent of these problems. One compendium of fault surveys [18], which examined 503 rooftop air-conditioning units in 181 buildings in five states in the Western U.S. from 2001-2004, found that the airflow was out of the specified range in approximately 42% of the units surveyed. A separate study [19] of 4,168 commercial air-conditioners in California reported that 44% of the surveyed units had airflow that was out of specifications. Studies of 29 new homes in Washington State [20] found that average duct leakage rates to the exterior ranged from 687 to 140 cubic feet per minute (CFM). Extrapolating from such fault surveys, one estimate for the total energy consumed by duct leakage is $5 billion/year [21].

When "failure is not an option," the performance of important electro-mechanical loads on mission-critical systems like warships or power plants is often tracked by dedicated monitoring equipment [22]. An extensive sensing network can provide obvious advantages for fault detection, diagnosis, and prognosis. However, a large sensing network can be expensive and difficult to maintain.

Smart Grid and Smart Meter initiatives hope to allow energy providers and consumers to intelligently manage their energy needs through real-time monitoring, analysis, and control of electrical power usage. The U.S. Department of Energy has identified "sensing and measurement" as one of the "five fundamental technologies" essential for driving the creation of a "Smart Grid" [23]. The methods described in this paper could be used to provide detailed energy score keeping and diagnostic measurements for motors for new metering schemes. These methods can be used by a non-intrusive load monitor (NILM) that determines the operating schedule of major electrical loads from measurements taken from an aggregate power feed serving multiple loads [24].

II. NILM Background

The non-intrusive load monitor has been demonstrated [25–28] as an effective tool for evaluating and monitoring electro-mechanical systems through analysis of electrical power data. The power distribution network can be pressed into "dual-use" service, providing not only power distribution but also a diagnostic monitoring capability based on observations of the way in which loads draw power from the distribution service. A key advantage of the non-intrusive approach is the ability to reduce sensor count by monitoring collections of loads.

Non-intrusive electrical monitoring has been described in [29, 30] among other publications. The systems that are described in these papers can be split into two broad categories: transient and steady-state approaches. The transient approach [30] finds loads by examining the full detail of their transient behavior. Reference [25] describes a platform for transient-based non-intrusive load monitoring appropriate for many applications.

The NILM detects the operation of individual loads in an aggregate power measurement by preprocessing measured current and voltage waveforms to compute spectral envelopes [31]. Spectral envelopes are short-time averages of the line-locked harmonic content of a signal. These spectral envelopes may be recognized as the coefficients of a time-varying Fourier series of the current waveform. For transient event detection on the ac utility, the time reference is locked to the line so that fundamental frequency spectral envelopes correspond to real and reactive power in steady state. Higher spectral envelopes

978-1-4244-4783-1/10/$25.00 ©2010 IEEE

correspond to line frequency harmonic content. A high performance transient event detection algorithm [30, 32] is available to disaggregate the fingerprints or spectral envelope signatures of individual loads in the aggregate measurement.

As will be shown below, subtle harmonics associated with the rotor of a motor are generally not found at integer multiples of the line frequency, although they may be spaced periodically in multiples of the line frequency. These rotor frequency harmonics, if detected, can be used to determine the operating speed of a motor. A NILM could provide this information by first detecting the activation of a motor of interest in the observed, line-locked spectral envelopes. Special attention can then be paid to the aggregate current frequency content just before and just after a turn-on transient to identify key harmonics that are indicative of rotor speed, and also pathological conditions in the motor.

III. Overall Block Diagram

This paper will introduce a new algorithm that can detect the speed-related slot harmonics in the NILM environment. The block diagram for this algorithm is shown in Fig. 1.

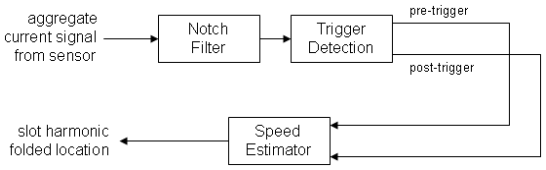

Fig. 1. Block diagram illustrating the processes of the algorithm. The important blocks include a notch filter, a trigger detection block and the final speed-estimation block.

A line-frequency notch filter improves the resolution of the relevant range of the input current. A pre-trigger and post-trigger detection block creates two streams of data from the output of the notch filter. Afterward, the outputs are used to estimate the speed for the corresponding motor.

IV. Rotor Slot Harmonics

Rotor slot harmonics are widely used in speed detection algorithms. Other harmonics appear in the stator current of a motor which often make the task of searching for these rotor slot harmonics more difficult. Motors can experience various kinds of mechanical failures or faults that inject their own set of harmonics into the stator current. The utility line supplying current to the stator may have its own distortions that present troublesome harmonics, especially in the NILM environment.

Rotor slot harmonics present in the stator current of a motor arise from the interaction between the permeance of the machine and the magnetomotive force (MMF) of the current in the stator windings. As the motor turns, the rotor slots alter the effective length of the airgap sinusoidally thereby affecting the permeance of the machine. This sinusoidal behavior is seen in the flux, which is the product of the MMF and the permeance across the airgap. The odd harmonics present in the stator current introduce additional harmonics. Static and dynamic eccentricity harmonics also appear in the stator current as the rotor turns irregularly in relation to the stator.

The slot harmonics, including the principal slot harmonic (PSH), are located at frequencies

$$f_{sh} = f\left[\left(kR + n_d\right)\frac{1-s}{p} + \nu\right] \tag{1}$$

where f is the supply frequency; $k = 0, 1, 2...$; R is number of rotor slots; $n_d = 0, \pm 1, ...$ is the order of rotor eccentricity; s is the per unit slip, p is the number of pole pairs and $\nu = \pm 1, \pm 3, ...$ is the stator MMF harmonic order [5, 33].

Previous research has been done to study the effects of mechanical faults on the stator current spectrum [6–17, 34]. These faults, including broken rotors bars, damaged bearings, rotor eccentricity, rotor asymmetry, bearings failures, and shaft speed oscillations, produce distinct harmonics in the current spectrum. One mechanical fault of interest is the shaft speed oscillation, which can be enhanced when an imperfectly balanced fan is attached to the motor shaft. The frequencies of interest [8] are predicted by

$$f_{sso} = f\left[k\left(\frac{1-s}{p}\right) \pm \nu\right].$$

These harmonics from the shaft speed oscillations are present in the stator current, complicating the detection of the principal slot harmonics.

The ac utility line is a potentially distorted sinusoid containing only the fundamental frequency f and harmonic multiples of this frequency. Depending on the time of day, the amount of loading on the utility line can vary substantially and can cause large distortions on the utility line. Also, line impedences create voltage distortions at frequencies determined by other loads in the system. These distortions, like the mechanical faults, introduce extra harmonics on the current spectrum.

A substantial amount of literature makes use of Eq. (1) for speed detection [1–3, 5, 35, 36]. The current spectrum of a motor with its slot harmonics Eq. (1) are shown in Fig. 2 for different values of ν. The motor used was a three-phase machine with $R = 48$ rotor slots and $p = 3$ pole pairs loaded by a dynomometer to run at $s = 0.0171$ or 1180 rpm. Typically, the slot harmonics with $k = 1$ and with $n_d = 0$ are the most pronounced in the current spectrum [1, 37]. For a given n_d, the slot harmonics differ exactly by $2f$ in Eq. (1).

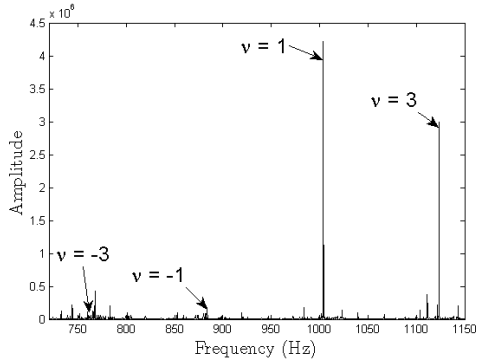

Fig. 2. Slot harmonics for a motor with the following parameters: f=60, k=1, R=48, n_d=0, $s = 1.71\%$ or 1180 rpm. The harmonics shown in the figure are labeled with the corresponding value of ν.

Analog techniques [35, 36] have been implemented to track these harmonics. The performance of these approaches can be limited in terms of accuracy, linearity, resolution, speed range, or speed of response [4]. Any analog filtering can require extremely complex circuitry and any output signal can be corrupted by noise. Digital techniques employing the Fast Fourier Transform (FFT) were developed [2] to overcome the flaws in the analog methods. These FFT methods were limited by the uncertainty principle, i.e. the trade-off between high frequency resolution and the response time to changes of speed that deteriorates with long data records. Parametric estimations [1, 3, 5] of the current spectrum were used to overcome the limitations of FFT but they require digital filters which make these methods less robust than the FFT. With a high stator frequency, the longer computations times can reduce any advantage these parametric methods may have over the FFT.

Some research has been done to combine the FFT and parametric estimation methods [1, 5]. In [1], the techniques do a successful job in tracking the slot harmonics in estimating speeds in a controlled environment. The authors make use of the periodicity of the slot harmonics by aliasing the spectrum such that these harmonics line up to increase detectability. We observe that the principal slot harmonic (PSH) is the most pronounced slot harmonic in the motors used in our experiments. The methods in this paper, therefore, will only search for the PSH, which simplifies the complexity of the algorithm.

There are certain trade-offs that must be made when deciding on the proper methods for detecting these speed-dependent rotor slot harmonics. The choices are often dictated by the practical setting.

V. Data Acquisition

NILM experiments from previous research collect data from a current sensor with only analog filtering for anti-aliasing. There is a large 60 Hz line frequency component that dominates the current signal, making detection of the smaller slot harmonics more difficult. To improve the detectability of the harmonics, a 60 Hz notch filter is implemented to remove the large line frequency component before the data acquisition hardware in the NILM samples the current.

In Fig. 3, the stator current signal is sent through a 60 Hz notch filter. The output is amplified by a gain stage and later filtered by a passive antialiasing filter. The output buffer drives the input of the NILM data acquisition hardware. The notch filter stage allows for improved signal detectability of the smaller slot harmonics. By removing the large dominant line frequency, the smaller harmonic signals can then be amplified, increasing the overall signal-to-noise ratio by reducing the effect of quantization noise in the ADC of the NILM.

VI. Practical Limitations on Slip

For high efficiency induction motors, the slip s usually does not exceed 5% and possibly less. This assumption leads to interesting simplifications when searching for the principal slot harmonic (PSH). The PSH refers to the slot harmonic with $\nu = 1$, $k = 1$, and $n_d = 0$ in Eq. (1) and is used in speed detection algorithms since it is often the most pronounced [1, 37]. The slot harmonics for different values of ν differ by $2f = 120$ Hz. If the principal slot harmonic was confined to a 120 Hz window under these practical limitations of slip, there would be no ambiguity in determining the window of the PSH.

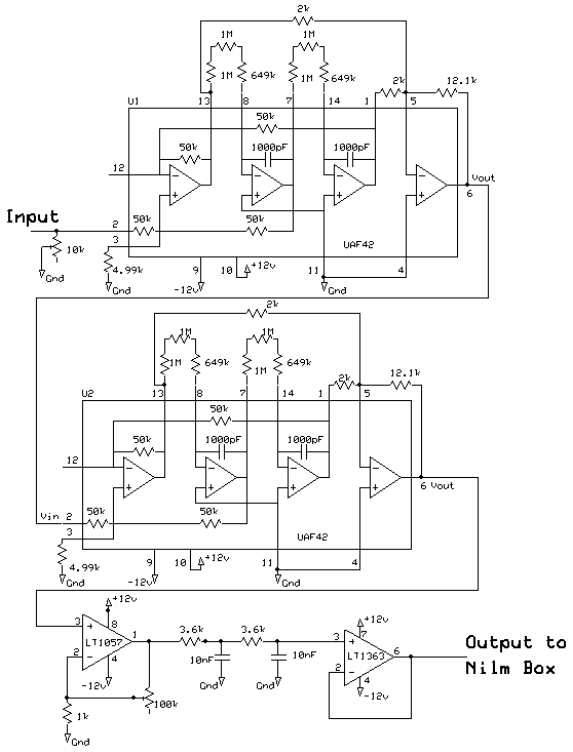

Fig. 3. Schematic of the 60 Hz notch filter circuit. The circuit notches the 60 Hz frequency, amplifies the signal and sends the signal through an antialiasing filter.

TABLE I
Maximum Slip for Unambiguous Speed Estimation for Several Values of R and p

	p			
R	1	2	3	4
16	0.1247	0.2494	0.3742	0.4989
20	0.0997	0.2000	0.3000	0.4000
24	0.0833	0.1667	0.2492	0.3333
28	0.0714	0.1428	0.2142	0.2856
32	0.0622	0.1244	0.1875	0.2489
34	0.0586	0.1172	0.1758	0.2344
40	0.0500	0.1000	0.1500	0.1989
44	0.0453	0.0906	0.1358	0.1811
48	0.0417	0.0833	0.1250	0.1667
52	0.0383	0.0767	0.1150	0.1533
56	0.0356	0.0711	0.1067	0.1422
60	0.0333	0.0667	0.1000	0.1333

For example, Table I tabulates the maximum slip for different values of R and p for which the PSH would be confined to a 120 Hz window.

For a motor with $R = 60$ and $p = 1$, a maximum slip of $s = 0.033$ would need to be assumed in order to constrain the PSH to a 120 Hz wide window. This assumption would be unreasonable because it would be possible for the motor to be

running with a slip of 0.04. In this situation, there would be some ambiguity in determining in which window the PSH lies. On the other hand, a motor with $R = 48$ and $p = 3$ can have a maximum slip of $s = 0.125$ to unambiguously determine the window of the PSH. This slip satisfies any reasonable low-slip assumptions.

VII. Speed Estimation via Slot Harmonics

Using a "low-slip" assumption in which the PSH is restricted to a single 120 Hz wide frequency window, this section will describe the application of the slot harmonics in determining speed of operation just after startup in a multi-load/multi-motor environment. To demonstrate the effectiveness of the algorithm, the speed estimation method was conducted with the following two motors. The first motor (Motor 1) was a three-phase motor from an HVAC evaporator in an air-handling unit. Motor 1 had $R = 48$ rotor slots and $p = 3$ pole pairs. The second motor (Motor 2) is a single-phase line-to-line machine from a fresh-air ventilation unit with $R = 34$ rotor slots and $p = 1$ pole pairs.

Consider an illustrative example in Fig. 4 in which the transient responses of induction motors are shown as they turn on and off. The region labeled A in 4(a) is when Motor 1 (the evaporator motor) turns on. Zooming in on Region A shows the transient response of Motor 1 as shown in Fig. 4(b). The region labeled B marks the region in which Motor 2 turns on so that both motors are running. The spectral envelope corresponding to "real" power as calculated by the NILM is shown in Fig. 5.

For the motors used in these experiments, Table I confirms that they satisfy the low-slip assumption. The PSH for Motor 1 will be between 900 Hz and 1020 Hz while the PSH for Motor 2 will be between 1980 Hz and 2100 Hz using Eq. (1).

As Motor 1 turns on, the NILM characterizes this new load from its transient turn-on response and spectral envelope. The aggregate current frequency contents before and after this transient event are recorded and are used to estimate the speed of Motor 1.

The window of interest to locate the PSH for Motor 1 is shown in Fig. 6(a). Using 5 seconds of current data, sampled at 7800 Hz, the location of the PSH can be estimated to be 993 Hz by finding the location of the maximum value within the window. Using Eq. (1), the speed can be estimated to be 1166.25 RPM.

By simply taking the maximum value within the PSH window, the resolution of the estimate is limited to the size of the FFT frequency bins, which is determined by the total duration of sampling. The estimate of the PSH (and the motor's speed) can be refined even further. As shown in Fig. 6(b), the energy of the PSH is actually spread over several frequency bins implying that there is not enough resolution to determine the PSH precisely [38]. One way to obtain finer resolution would be to sample data over a longer interval, which is unattractive as the speed of the motor may vary during the interval. A different approach, is to use the information in the frequency bins near the peak.

Consider the illustrative example in Figure 7 of the FFT of a pure sinusoid wave with a frequency of 994.34 Hz. In

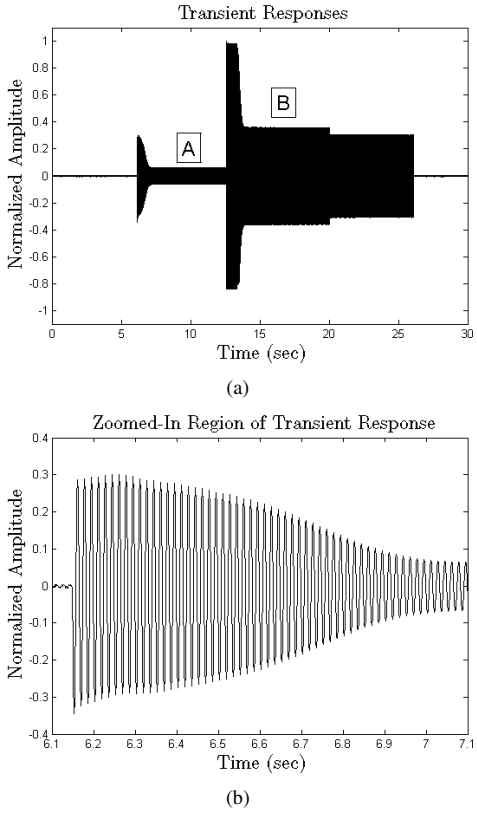

Fig. 4. In (a), the current data stream with transient responses. The turn-on transient when Motor 1 turns on (Region A) is shown in (b)

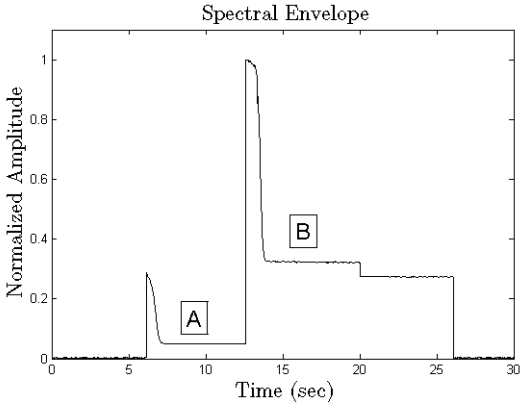

Fig. 5. Spectral envelope calculation.

Fig. 7(a), the FFT of 5 seconds of this pure sine wave is shown. Compare this result with that of Fig. 7(b) and Fig. 7(c) in which the data length is reduced to $.5$ seconds and $.05$ seconds respectively. The energy of the signal is spread over an increasingly wider frequency band as the data duration decreases.

When dealing with the short, $.05$ second long data, each bin of the resulting FFT is 20Hz wide. Estimating the frequency (994.34 Hz, in this example) from simply looking at the peak within a window could only hope to provide resolution of 20 Hz. The situation can be improved by producing $.05$ seconds

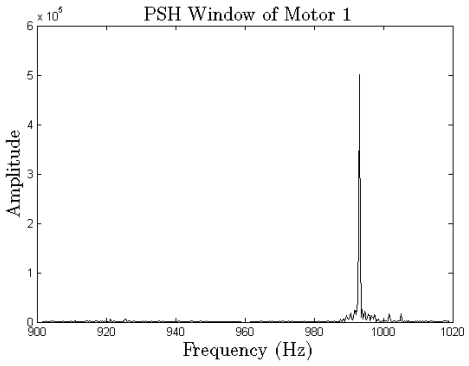

(a) Aggregate current spectrum w/ Motor 1 running.

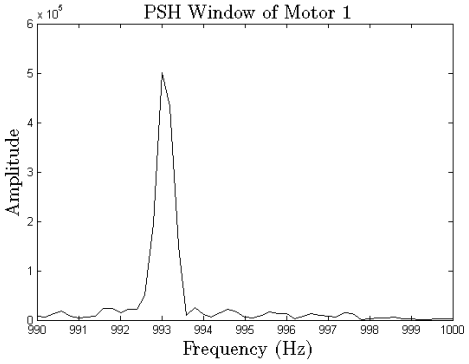

(b) Current spectrum with w/ Motor 1 running. The frequency content of the PSH is spread over multiple bins.

Fig. 6. In (a), the frequency content of the PSH is actually spread over several frequency bins as shown in Fig. 6(b).

of data from each of a family of sine waves with frequencies in the neighborhood of the observed peak. An optimization routine can pick the frequency of a sinusoid whose FFT is the best fit (in the minimum mean square sense) for the observed data over the entire frequency neighborhood around the peak. This routine makes the assumption that there is only a single, pure sinusoid in the window responsible for all observed frequency content. In this case, the optimization routine selects exactly 994.34 Hz as there is no noise to corrupt the data. Essentially, a finer estimate can be made by using the energy that has spread over several bins as opposed to only making use of the content in just one bin.

This same idea can be applied to the actual data taken from Motor 1. All of the following data is taken at a sampling frequency of 7800 Hz. Using the full 5 seconds length of data, the estimate of the PSH for Motor 1 is 993 Hz. A speed estimate of 1166.250 RPM is then calculated from this estimate of the PSH. The results of applying the optimization routine to shorter lengths of data are shown in Fig. 8.

The frequency content for 0.5 seconds of data of Motor 1 near the PSH is shown by the solid line in Fig. 8(a). The optimization routine finds the the frequency of a sinusoid whose FFT best matches the observed data, in this case 992.7 Hz. Again, the optimization routine is making the assumption that there is only a single, pure sinusoid responsible for all observed frequency content. The dotted line in Fig. 8(a) is the

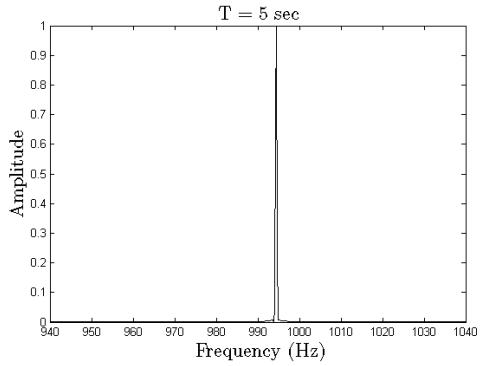

(a)

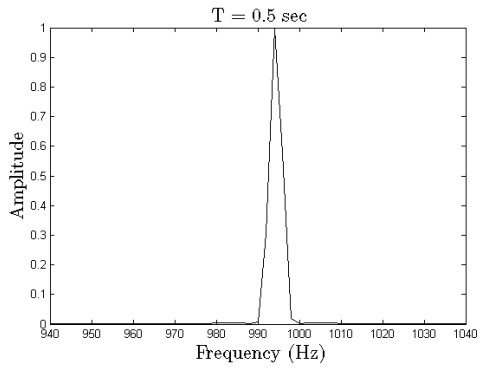

(b)

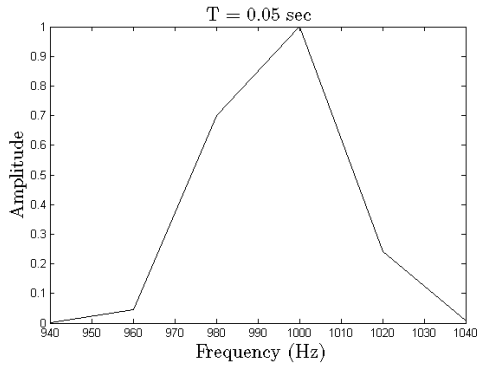

(c)

Fig. 7. In (a), the FFT is shown for the sinusoid with a sampling time of 5 seconds. The energy in the peak spreads out over several frequency bins as the sampling duration decreases as shown in (b) and (c).

FFT of a 0.5 second sinusoid with a frequency of 992.7 Hz. The FFT of this sinusoid closely matches that of the observed data (solid line) in the region of interest. A speed estimate of 1165.870 RPM is then calculated from the optimized estimate of the PSH. This is repeated for 0.05 seconds of data in Fig. 8(b). The optimized PSH is 992.08 Hz and the corresponding speed estimate is 1165.100 RPM.

This optimization routine maintains accurate speed estimates despite using a shorter duration of data. By utilizing more data from the nearby frequency bins, and the assumption that only a single sinusoid is responsible for the observed frequency content, the routine can predict reliable speed estimates on a smaller data set. Table II displays the results of

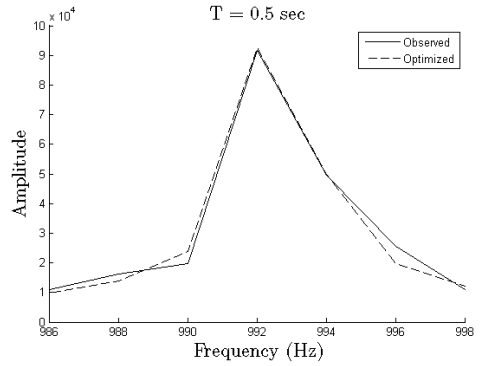

(a) The observed PSH is shown in the solid line. The dotted line is the FFT of the best-fit sinusoid. The sampling time is 5 seconds.

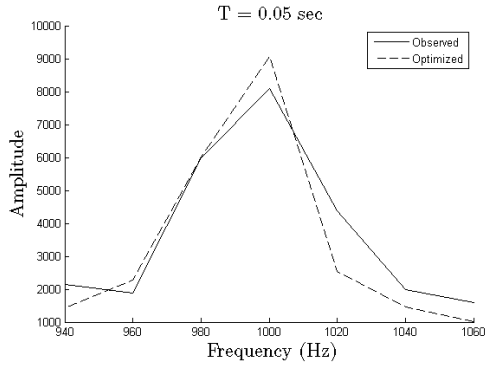

(b) The observed PSH is shown in the solid line. The dotted line is the FFT of the best-fit sinusoid. The sampling time is 0.5 seconds.

Fig. 8. The observed PSH and FFT of the best-fit sine waves for a sampling time of $T = 5$ seconds (a) and $T = 0.5$ (b).

TABLE II
OPTIMIZATION ROUTINE PSH AND SPEED ESTIMATES AT DIFFERENT SAMPLING TIMES

T (sec)	Line Cycles	PSH (Hz)	Speed (RPM)
5	300	993.080	1166.350
3	180	992.929	1166.161
1	60	992.760	1165.950
0.5	30	992.700	1165.870
0.1	6	992.960	1166.200
0.05	3	992.080	1165.100
0.0333	2	997.200	1171.500
0.0166	1	990.140	1162.675

the optimizing routine for different sampling times.

The speed detection algorithm runs as new loads turn on. When Motor 2 turns on, there are scenarios that may complicate tracking speeds. If both motors are identical in parameters, the worst case scenario would have both motors running at the same speed. In such a case, the principal slot harmonic (PSH) of each motor would be at the exact same location. To prevent this, if possible, the motors can be selected so that such a scenario could not occur. In this experiment, the parameters of the motors were chosen such that the PSH of each motor would appear in separate windows.

Also complicating speed detection, the utility line has its own set of harmonics which are visible in the current spectrum. The 17th harmonic at 1020 Hz could be troublesome in trying to identify the PSH of Motor 1. Fortunately, as these undesirable harmonics are located at integer multiples of 60 Hz, we can easily filter them out using the digital filter $y[n] = x[n] - x[n - N]$ where N is the number of sample points per 60 Hz line cycle (in this paper, all data is sampled at 7.8 KHz, which corresponds to $N = 130$). This filter will notch out all the integer multiples of the line frequency.

One problem, which shows up in this experiment as Motor 2 turns on, is the addition of eccentricity harmonics [6]. Motor 2 is loaded with a fan which exacerbates these eccentricities. Figure 9(a) shows the window of interest for the PSH of Motor 1 when both motors are running. In this paper, the motors examined had slot harmonics that are larger in amplitude than any of the eccentricity harmonics. Tracking these eccentricity harmonics may be possible by first estimating the speed of the eccentric motor. Once the slip is estimated, all possible eccentricity harmonics can be tabulated and tracked. Changes in the observed amplitudes of these eccentricity harmonics can be used to diagnose the health of the motor. Also, the above algorithm can use knowledge of eccentricity harmonics to make better speed predictions by properly including the effects of the eccentricity harmonics in the observed frequency content. The PSH for Motor 2 was determined to be between 1980 and 2100 Hz. The current spectrum at these frequencies is shown in Fig. 9(b). The optimized PSH for Motor 2 is estimated at 2046.28 Hz which corresponds to 3505.20 rpm.

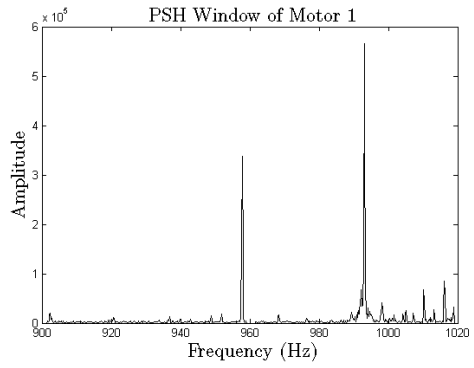

(a)

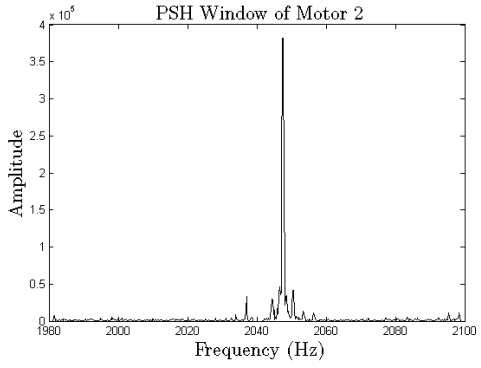

(b)

Fig. 9. Aggregate current spectrum with both motors running. In (a), the current spectrum in the PSH window of Motor 1 and in (b), the spectrum in the PSH window of Motor 2.

VIII. Airflow Diagnostics Application

As an example of the utility of knowing motor speed in addition to power consumption for load diagnostics, consider ventilation systems in residential or commercial buildings. A system that is able to monitor the state of airflow and detect faults in ventilation systems would fulfill a significant need in contemporary buildings, due to the prevalence of airflow faults. One widely used ventilation system employs air-side distribution systems for air-conditioning units typically called air handlers, air handling units, or AHUs. A picture and a visual representation of the AHU used in [39] are shown in Fig. 10.

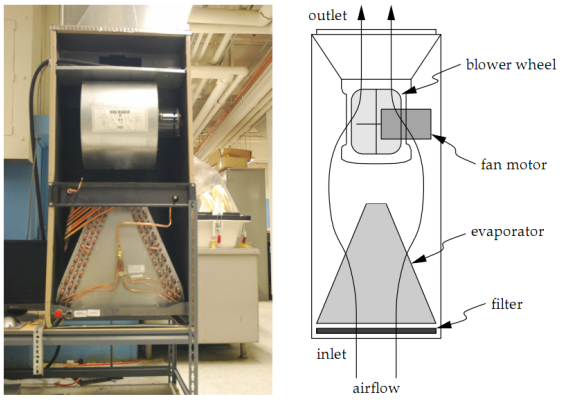

Fig. 10. Schematic diagram and picture of air handler.

A common fault in these systems occurs when the filter to the air handler, or the evaporator itself, is clogged, causing the airflow through the fan to be reduced. While the most notable effect of such a fault will be on the reduction in the air delivered to the building occupants, this fault can also potentially chill the volume of air flowing through the AHU further than is intended. A dramatically reduced flow rate could also affect the system health of the overall air-conditioning system, and of the compressor more specifically; if little air is traveling through the evaporator, the cooling load on the evaporator could be substantially reduced, causing the amount of refrigerant evaporated in the evaporator to be much smaller than required by the design specifications. This could potentially result in liquid refrigerant entering the compressor through the suction line, causing the ingestion of liquid refrigerant by the compressor, permanently damaging it. Also, the accumulation of material on the filter or the evaporator can also effect the health of building occupants. The accumulation of bacteria or mold on these surfaces can affect people breathing the air.

The architecture of the airflow estimation method in [39] is dependent upon the estimation of three related quantities: the mechanical torque applied to the fan τ_f , the speed of the fan blades ω_f , and the fan curve at the operating point of the fan. Since the fan curve is measured empirically by the manufacturer, it is necessary to develop a method to determine ω_f and τ_f from the motor electrical variables V_m and I_m. The block diagram below shows the estimation scheme employed in [39].

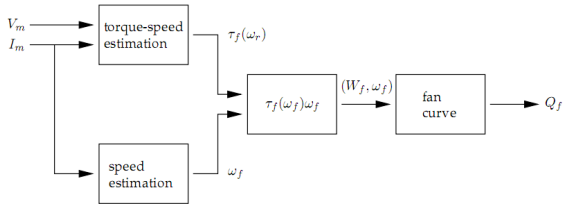

Fig. 11. Structure of the airflow estimation method.

To identify the airflow Q_f, the speed ω_f and the torque-speed curve $\tau_f(\omega_r)$ are first estimated independently from the electrical variables. The methods introduced in this paper describe a way that the speed ω_f of the fan blades can be non-intrusively estimated. The torque $\tau_f(\omega_r)$ at the motor's present operating point can then be identified by monitoring the voltage and current supplied to the fan. With these estimates of ω_f and τ_f, the operating mechanical shaft power W_f can be identified. The mechanical power and the operating speed are then used to identify the point on the fan curve that describes the fan's current state, thereby generating an estimate of the volumetric airflow Q_f through the fan. An estimate of Q_f (cfm) can be recorded many times after many starts of the fan. These estimates can be collected in a histogram and tracked and trended over time as shown in Fig. 12 [39] for diagnostic purposes.

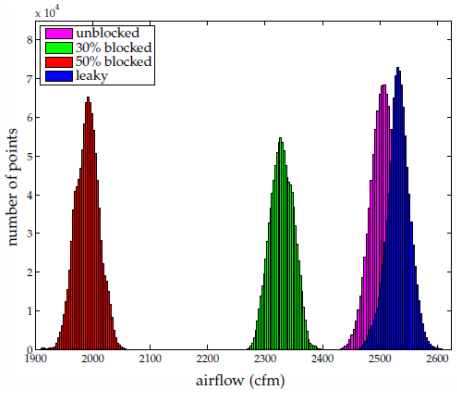

Fig. 12. Illustration of airflow detectability using torque-speed curves that are generated from minimization against the motor current and the torque-speed curve, as collected for each blockage condition.

Fig. 12 shows experimentally derived histograms for the airflow of the AHU when the intake filter is unblocked, 30% blocked, 50% blocked and leaky. As expected, the airflow estimates are indicative of the mechanical condition of the AHU.

IX. Conclusions

It is often reasonable to assume that basic information about an electro-mechanical plant will be available for residential and industrial applications. For example, the torque-speed curve of an air handling motor or pump is often known, or could be obtained by or from a manufacturer. Similar information, e.g., a fan curve relating shaft power and speed to air flow, can be found for common fans and, similarly,

for pump heads. The experimental results presented here demonstrate how a non-intrusive load monitor can determine electrical power and mechanical shaft speed from a reasonably chosen aggregate power measurement where other loads may also be operating. In situations where data like torque-speed curves are known *a priori*, a NILM could use this information along with its measurements of electrical power consumption and motor operating speed to perform fault detection and diagnostics on critical energy consumers like air conditioning and air handling systems.

This paper illustrates how the known behavior of motor harmonics could be exploited with reasonable assumptions about operating conditions to estimate speed in a non-intrusive setting. Spectral envelope computations are used to characterize the operating schedule of loads as then turn on. Once recognized as "on", the current before and after the transient can be analyzed to estimate the speed of the new motor joining the collection of operating loads on the monitored service. A fine estimate of speed can be calculated by employing an optimization routine to find the optimal frequency of a sinusoid that closely matches the spectral content of the observed data. This optimization routine allows for smaller sampling windows to obtain desirable frequency resolution. This technique can be extended to estimate the speeds of multiple motors from on aggregate current signal.

Of course, an unfortunate collection of loads could hinder the NILM's ability to detect operating speeds. In critical situations where non-intrusive monitor is desirable, motors might be selected during the design of a plant to enhance detection.

X. Acknowledgments

This work was supported in part by the MIT SeaGrant program, The Grainger Foundation, the National Science Foundation and the BP-MIT Research Alliance.

References

[1] K. D. Hurst and T. G. Habetler, "Sensorless Speed Measurement Using Current Harmonic Spectral Estimation in Induction Machine Drives," *IEEE Trans. Power Electron.*, vol. 11, no. 1, pp. 66–73, 1996.

[2] A. Ferrah, K. G. Bradley, and G. M. Asher, "Sensorless Speed Detection of Inverter Fed Induction Motors Using Rotor Slot Harmonics and Fast Fourier Transform," vol. 1. IEEE Power Electronics Specialist Conference, Jun. 29 - Jul. 3 1992, pp. 279–286.

[3] A. Ferrah, P. J. Hogben-Laing, K. J. Bradley, G. M. Asher, and M. S. Woolfson, "The Effect of Rotor Design on Sensorless Speed Estimation Using Rotor Slot Harmonics Identified by Adaptive Digital Filtering Using The Maximum Likelihood Approach," in *Industry Applications Conference, 1997. Thirty-Second IAS Annual Meeting, IAS'97., Conference Record of the 1997 IEEE*, vol. 1, Oct. 1997, pp. 128–135.

[4] A. Ferrah, K. J. Bradley, P. J. Hogben-Laing, M. S. Woolfson, G. M. Asher, M. Sumner, J. Cilia, and J. Shuli, "A Speed Identifier For Induction Motor Drives Using Real-Time Adaptive Digital Filtering," *IEEE Trans. Ind. Applicat.*, vol. 34, no. 1, pp. 156–162, 1998.

[5] K. D. Hurst and T. G. Habetler, "A Comparison of Spectrum Estimation Techniques For Sensorless Speed Detection in Induction Machines," *IEEE Trans. Ind. Applicat.*, vol. 33, no. 4, pp. 898–905, 1997.

[6] M. E. H. Benbouzid, "A Review of Induction Motors Signature Analysis as a Medium For Faults Detection," *IEEE Trans. Ind. Electron.*, vol. 47, no. 5, pp. 984–993, 2000.

[7] G. B. Kliman, R. A. Koegl, J. Stein, R. D. Endicott, and M. W. Madden, "Noninvasive Detection of Broken Rotor Bars in Operating Induction Motors," *IEEE Trans. Energy Conversion*, vol. 3, no. 4, pp. 873–879, 1988.

[8] G. B. Kliman and J. Stein, "Methods of Motor Current Signature Analysis," *Electric Machines and Power Systems*, vol. 20, no. 5, pp. 463–474, 1992.

[9] S. Nandi, H. A. Toliyat, and X. Li, "Condition Monitoring and Fault Diagnosis of Electrical Motors - A Review," *IEEE Trans. Energy Conversion*, vol. 20, no. 4, pp. 719–729, 2005.

[10] N. M. Elkasabgy, A. R. Eastham, and G. E. Dawson, "Detection of Broken Bars in the Cage Rotor on an Induction Machine," *IEEE Trans. Ind. Applicat.*, vol. 28, no. 1 Part 1, pp. 165–171, 1992.

[11] W. T. Thomson and M. Fenger, "Current Signature Analysis to Detect Induction Motor Faults," *IEEE Ind. Appl. Mag.*, vol. 7, no. 4, pp. 26–34, 2001.

[12] R. R. Schoen, T. G. Habetler, F. Kamran, and R. G. Bartfield, "Motor Bearing Damage Detection Using Stator Current Monitoring," *IEEE Trans. Ind. Applicat.*, vol. 31, no. 6, pp. 1274–1279, 1995.

[13] R. R. Schoen and T. G. Habetler, "Effects of Time-Varying Loads on Rotor Fault Detection in Induction Machines," *IEEE Trans. Ind. Applicat.*, vol. 31, no. 4, pp. 900–906, 1995.

[14] R. R. Schoen, B. K. Lin, T. G. Habetler, J. H. Schlag, and S. Farag, "An Unsupervised, On-line System For Induction Motor Fault Detection Using Stator Current Monitoring," in *Conference Record of the 1994 IEEE Industry Applications Society Annual Meeting, 1994.*, 1994, pp. 103–109.

[15] M. E. H. Benbouzid, M. Vieira, and C. Theys, "Induction Motors' Faults Detection And Localization Using Stator Current Advanced Signal Processing Techniques," *IEEE Trans. Power Electron.*, vol. 14, no. 1, pp. 14–22, 1999.

[16] J. R. Cameron, W. T. Thomson, and A. B. Dow, "Vibration and Current Monitoring for Detecting Airgap Eccentricity in Large Induction Motors," *IEE Proceedings B [see also IEE Proceedings-Electric Power Applications] Electric Power Applications*, vol. 133, no. 3, pp. 155–163, 1986.

[17] H. Guldemir, "Detection of Airgap Eccentricity Using Line Current Spectrum of Induction Motors," *Electric Power Systems Research*, vol. 64, no. 2, pp. 109–117, 2003.

[18] A. Cowan, "Review of Recent Commercial Rooftop Unit Field Studies in the Pacific Northwest and California," New Buildings Institute, PO Box 653, White Salmon,WA, 98672, Tech. Rep., Oct. 8 2004.

[19] R. J. Mowris, A. Blankenship, and E. Jones, "Field measurements of air conditioners with and without TXVs," 2004.

[20] D. Hales, A. Gordon, and M. Lubliner, "Duct Leakage in New Washington State Residences: Findings and Conclusions," *ASHRAE Transactions-American Society of Heating Refrigerating Airconditioning Engineers*, vol. 109, no. 2, pp. 393–402, 2003.

[21] K. Srinivasan, "Measurement of Air Leakage in Air-Handling Units and Air Conditioning Ducts," *Energy & Buildings*, vol. 37, no. 3, pp. 273–277, 2005.

[22] *Field Demonstration of a Real-Time Non-Intrusive Monitoring System for Condition-Based Maintenance*. National Harbor, Maryland: Electric Ship Design Symposium, Feb. 2009.

[23] U. S. Department of Energy, "The Smart Grid: An Introduction," World Wide Web electronic publication. [Online]. Available: http://www.oe.energy.gov/1165.htm

[24] G. W. Hart, "Nonintrusive Appliance Load Monitoring," *Proc. IEEE*, vol. 80, no. 12, pp. 1870–1891, Dec. 1992.

[25] S. R. Shaw, S. B. Leeb, L. K. Norford, and R. W. Cox, "Nonintrusive Load Monitoring and Diagnostics in Power Systems," *IEEE Trans. Instrum. Meas.*, vol. 57, no. 7, pp. 1445–1454, Jul. 2008.

[26] J. S. Ramsey *et al.*, "Shipboard Applications of Non-Intrusive Load Monitoring," in *ASNE Conference on Survivability and Reconfiguration*, Feb. 2005.

[27] T. DeNucci, R. Cox, S. B. Leeb, J. Paris, T. J. McCoy, C. Laughman, and W. C. Greene, "Diagnostic indicators for shipboard systems using non-intrusive load monitoring," *IEEE Electric Ship Technologies Symposium*, pp. 413–420, Jul. 2005.

[28] W. Greene, R. J. S., R. Cox, and T. DeNucci, "Non-intrusive monitoring for condition-based maintenance," *Proc. ASNE Reconfiguration and Survivability Symposium*, Feb. 16 2005.

[29] S. B. Leeb, "A Conjoint Pattern Recognition Approach to Nonintrusive Load Monitoring," Ph.D. dissertation, Massachusetts Institute of Technology, Cambridge, MA, Feb. 1993.

[30] S. B. Leeb, S. R. Shaw, and J. L. Kirtley Jr., "Transient Event Detection in Spectral Envelope Estimates For Nonintrusive Load Monitoring," *IEEE Trans. Power Delivery*, vol. 10, no. 3, pp. 1200–1210, Jul 1995.

[31] S. R. Shaw, "System identification techniques and modeling for nonintrusive load diagnostics," Ph.D. dissertation, Massachusetts Institute of Technology, Cambridge, MA, Feb. 2000.

[32] R. Cox, S. B. Leeb, S. R. Shaw, and L. K. Norford, "Transient Event Detection For Nonintrusive Load Monitoring and Demand Side Management Using Voltage Distortion," Mar. 2006.

[33] S. Nandi, S. Ahmed, and H. A. Toliyat, "Detection of Rotor Slot and Other Eccentricity Related Harmonics in a Three Phase Induction Motor With Different Rotor Cages," *IEEE Trans. Energy Conversion*, vol. 16, no. 3, pp. 253–260, 2001.

[34] C. Hargis, B. G. Gaydon, and K. Kamash, "The Detection of Rotor Defects in Induction Motors," in *Proc IEE EMDA Conf, London*, 1982, pp. 216–220.

[35] M. Ishida and K. Iwata, "A New Slip Frequncy Detector of an Induction Motor Utilizing Rotor Slot Harmonics," *IEEE Trans. Ind. Applicat.*, pp. 575–582, 1984.

[36] D. S. Zinger, F. Profumo, T. Lipo, and D. W. Novotny, "A Direct Field-Oriented Controller for Induction Motor Drives Using Tapped Stator Windings," *IEEE Trans. Power Electron.*, vol. 5, no. 4, pp. 446–453, 1990.

[37] S. Nandi, "Modeling of Induction Machines Including Stator and Rotor Slot Effects," in *Industry Applications Conference, 2003. Conference Record of the 38th IAS Annual Meeting.*, vol. 2, 2003.

[38] A. V. Oppenheim, R. W. Schafer, and J. R. Buck, *Discrete-time Signal Processing*. Prentice Hall Englewood Cliffs, NJ, 1989.

[39] C. Laughman, "Fault Detection Methods for Vapor-Compression Air Conditioners Using Electrical Measurements," Ph.D. dissertation, Massachusetts Institute of Technology, Cambridge, MA, Sep. 2008.